Received: 8 May 2020 | Revised: 12 July 2020 | Accepted: 24 July 2020

DOI: 10.1002/qua.26434

FULL PAPER

International Journal of QUANTUM CHEMISTRY WILEY

The magnetic binary lithium clusters W_2Li_n (n = 15-19): A theoretical prediction of "di-superatomic molecules"

Lijuan Yan

College of Electronics and Information Engineering, Guangdong Ocean University, Zhanjiang, China

Correspondence
Lijuan Yan, College of Electronics and Information Engineering, Guangdong Ocean University, Zhanjiang 524088, China.
Email: ylj_gdou@126.com

Funding information
Special Foundation for Theoretical Physics Research Program of China, Grant/Award Number: 11847119

Abstract

Based on the super valence bond (SVB) model, a motif of face-sharing bi-tetrahexahedral superatomic molecules $M_1M_2@Li_{20}$ (M_1/M_2 = Ti and W) was recently constructed by fusion of two tetrahexahedral superatoms $Ti@Li_{14}$ and $W@Li_{14}$. Here, as an extension of the formation of molecules from superatoms, binary lithium clusters W_2Li_n (n = 14-19) are studied in conjunction with particle swarm optimization algorithm search and density functional theory calculations. The lowest-lying isomers of W_2Li_n (n = 15-19) with the magnetic moments of 0 to 3 μ_B are identified as superatomic molecules by analysis of their molecular orbitals and chemical bonding patterns, whereas the global minimum isomer of W_2Li_{14} does not possess the geometric structure of monomer. Via a lithium atom sequentially removed, a series of superatomic bond orders of 3, 3.5, 4, and 4.5 are exposed, reminiscent of classical chemical bonds. Meanwhile, many isosupermolecules are found in the low-energy structures, predicting the diversity assembly of superatom materials. Our results highlight the tremendous opportunities for molecules assembled by superatoms, which may be in favor of the designs of nanoparticles or functional materials in future according to the SVB model.

KEYWORDS

magnetic properties, multiple super bond, stability, superatomic molecular structures

1 | INTRODUCTION

Since 1984, the large peaks in the mass spectra of sodium clusters have been associated with their electronic shells.[1] Studies of stable clusters have aroused great interest, where an important focus is offering plentiful building blocks for cluster-assembled materials with the most promising tailored properties. The features of the assembled materials can especially be controlled while keeping the geometric structures of the building units unchanged. However, unlike the situation of atoms as building blocks, the structural integrity of cluster units is most probably distorted in the assembly, which then increases the complexity of materials assembled from clusters. Therefore, the stability of the chosen cluster units is of crucial importance for self-assembly into materials.

With unusual stability, superatoms have great potential as building blocks of multisuperatom molecules and condensed phase materials, for which both the orbital shapes of electronic states and the associated chemical properties are similar to those of elemental atoms.[2] For metal superatoms, their stability can be accounted for by the jellium model, where the motions of valance electrons are confined in an assumed uniform positive charge composed of the atomic nuclei and inner electrons.[3,4] Using this model, electronic shell closure occurs with electron counts of 2, 8, 18, 20, 34, 40, 58, etc. corresponding to the size clusters with large peaks in the sodium mass spectra. In 2009, the concept of superatoms was further extended to open-shell systems by the Khanna group, who found relatively localized orbitals and diffuse valence orbitals coexisting in

a cluster,[5] where the magnetic moment can be acquired via the orbitals localized at the sites of atoms, and the corresponding evidence of magnetic superatoms has been presented in experiment.[6]

As a precondition of selecting suitable cluster units, the identification of assembly motifs for the extended materials is another challenge. Notably, Cheng and Yang developed a new concept of a super valence bond (SVB),[7] with the basic idea being that the electronic shell closures for superatoms were achieved by sharing valence pairs and nuclei of superatoms and superatoms or atoms. Based on this model, the stability of some nonspherical mental clusters is well understood, such as $Au_{38}(SR)_{24}$, of which the Au_{23}^{9+}(14e) core can be deemed a superatomic molecule assembled by two icosahedrons.[8] Furthermore, Cheng et al. extended the conventional atom-atom quintuple bonding ($\sigma 2\pi 2\delta$) to the scope of the superatoms through the analyses of the MOs shapes and chemical bonding patterns of 26e $Li_{20}Mg_3$ and 30e $Li_{18}Mg_3Al_2$ clusters.[9] Many multisuperatom bonds, such as single, double, triple, and especially delta superatomic bonds, have been demonstrated to in superatomic molecules,[10–12] bridging the atom materials and cluster-assembled materials.

To comprehend the self-assembly from superatoms, we have constructed a series of D_{6d} symmetry tetrahexahedral lithium superatoms $TM@Li_{14}$ (TM = Sc, Ti, V, Y, Zr, Nb, Hf, Ta, and W).[13] Among them, the 18e $Ti@Li_{14}$ and the 20e $W@Li_{14}$ superatoms with the closed geometric and electronic shells are chosen as building blocks. By fusing two monomers along their C_6 axis, a face-sharing bi-tetrahexahedral motif with the properties of superatomic molecules is proposed, where the number of atoms shared by the two superatoms is up to six.[14] A question then arises regarding whether the formation of the superatomic molecules is coincidental or is certain. For a less compact cluster, could it be a superatomic molecule, and what makes it stable? Here, a universal description of the superatomic molecules is presented by using $W_2@Li_n$ (n = 14-19) clusters as the example. Possible low-energy structures are first investigated and are then systematically examined from the aspects of geometric structures, stability, electronic shells, and magnetic properties. With the reduction of the number of lithium atoms, the lowest-lying isomers of $W_2@Li_n$ (n = 15-19) still behave as superatomic molecules with spin magnetic moments of 0 to 3 μ_B, and the electronic structures of their corresponding building units resemble those of magnetic superatoms VLi_n (n = 8-13).[15] Moreover, a broad pattern of superatom bonding is discovered between the two building superatoms.

2 | COMPUTATIONAL METHODS

In search of the low-lying isomers of $W_2@Li_n$ (n = 14-19) clusters, the particle swarm optimization (PSO) algorithm interfaced with Gaussian is performed, which is efficient in cluster structure prediction and has been implemented in the Crystal structure AnaLYsis by Particle Swarm Optimization (CALYPSO) package.[16] For the initial generation, its structures are randomly produced, while 60% of the structures of the other generations are derived from previous generations, evolved by PSO, and 40% are new and generated randomly. Each generation contains 50 structures. The search convergence has been achieved by 50 generations of completed structural candidates. Low-lying structures with an energy difference of less than 2 eV of the global minimum isomer are reoptimized at the density functional theory (DFT) level using Gaussian 16.[17] The spin multiplicities (SMs) are considered during the reoptimization procedure, including at least four possible SMs of 1, 3, 5, 7, ..., or 2, 4, 6, 8, ... for even or odd electron clusters, respectively. Correspondingly, the SMs with the lowest energy are then identified as their ground states. All the structures are confirmed as true local minima without any imaginary frequency.

Due to the availability of the SDD basis set in binary lithium clusters $M@Li_{16}$ (M = Ca, Sr, Ba, Ti, Zr, Hf)[18] and comparison with our previous work of $W_2@Li_{20}$,[14] it is continually adopted. The calculations on $W_2@Li_n$ (n = 14-19) are performed with a combination of three functionals, namely, pure functional PW91,[19] meta-GGA functional M06-L,[20] and hybrid functional TPSSH,[21] which have been proven to be the most valid for the lithium clusters system.[22,23] The structures of molecular orbitals (MOs) and chemical bonding orbitals are completed by Multiwfn_3.6.[24]

3 | RESULTS AND DISCUSSION

3.1 | Low-energy isomers of $W_2@Li_n$ (n = 14-19) clusters

Using the PSO algorithm, several isomers of $W_2@Li_n$ (n = 14-19) are located, and only the first four lower-lying structures are presented in Figure 1. Conventionally, each isomer of $W_2@Li_n$ (n = 14-19) is labeled as n.X, where n denotes the number of Li atoms with a range from 14 to 19, and X (= A, B, C, D) corresponds to the several low-lying isomers arranged by their increasing relative energy for the calculations at the PW91/SDD level. Similar to $W_2@Li_{20}$, all the most stable isomers of $W_2@Li_n$ (n = 15-19) clusters can be viewed as the assembly of two units along their axis.

3.2 | $W_2@Li_{19}$

The geometric structural motif shared with a six-membered Li ring is used for $W_2@Li_{19}$ (19.A), but its point group becomes C_s due to a reduction of one lithium atom compared with $W_2@Li_{20}$. Accordingly, the two units of $W_2@Li_{19}$ are inequivalent, possessing 14 atoms and 15 atoms, respectively,

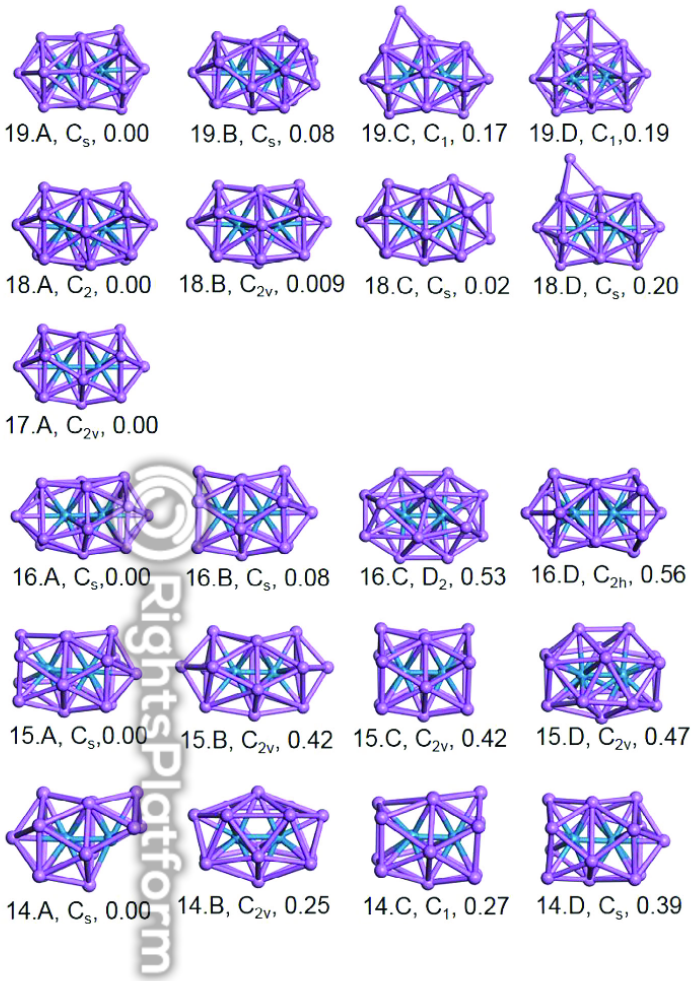

FIGURE 1 The geometric structures, symmetry, and relative energies (eV) for the first four low-lying isomers of W_2Li_n (n = 14-19) at the PW91/SDD level

where the dimer is formed by a top-to-top assembly of monomers on their six-membered sides as shown in Figure 2. The second lower-lying isomer (19.B) is developed with the formation of a five-membered Li ring through a top-to-side assembly of 15-atom and 14-atom units. The relative energy of 19.B is 0.08 eV higher than that of the 19.A isomer. However, the two isomers of 19.B and 19.A exhibit similar electronic configurations (Figure S1). Based on the concept of isosupermolecules that were developed by Yang and co-workers,[25] 19.B can be considered an isosupermolecule of 19.A. For 19.C and 19.D, there is one or two lithium outside their surface cages, with energy being higher by about 0.17 and 0.19 eV, respectively.

3.3 | $W_2@Li_{18}$

With two lithium atoms removed, the lowest-energy isomer of $W_2@Li_{18}$ (18.A) remains in the six-membered face-sharing mode, of which the building blocks are two identical units, $W@Li_{13}$ and a C_{2v} symmetry cluster with asymmetrical faces composed by the direct face connection of two capped five- and six-membered rings (Figure S2). The 18.A isomer is formed by the face fusion of two $W@Li_{13}$ on their six-atom ring side. The same formation pattern is observed in the 18.B isomer, where the six-membered ring is slightly curved, and its energy is 0.009 eV higher than that of the most stable isomer. The five-membered sharing structure appears in the third low-lying isomer of 18.C that is 0.02 eV higher in energy, which can be viewed as a top-to-side assembly of a 13-atom unit and a 14-atom unit. The C_s symmetry 18.D isomer is similar to $W_2@Li_{19}$ (19.C) with one lithium atom removed from the middle of the six-membered ring, and this structure is less stable than 18.A by 0.20 eV. Structurally, the isomers 18.B and 18.C are isosupermolecules of 18.A (electronic configurations not shown for analogies).

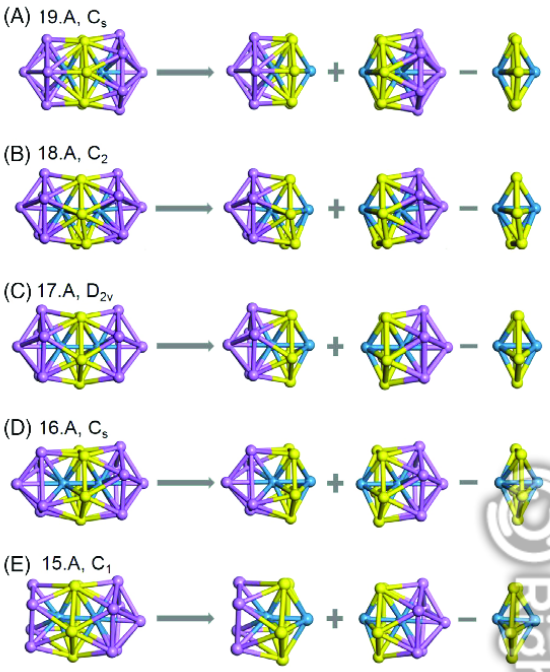

FIGURE 2 Schematic diagram of di-superatomic model for the lowest-energy structures of W_2Li_n (n.A, n = 15-19)

3.4 | $W_2@Li_{17}$

Different from $W_2@Li_n$ (n = 18-20, n.A), the most stable isomer of $W_2@Li_{17}$ (17.A) is characterized by a five-membered face-sharing mode, of which the building block $W@Li_{12}$ is an I_h symmetry icosahedron composed of 12 equal pentagons. Regardless of how the two $W@Li_{12}$ units are merged, for instance, using the fusion of top-to-top and side-to-side or their mixture, the 17.A isomer with the symmetry of C_{2v} can still be produced. In addition, the generation process can be regarded as removing the distorted lithium atom in the six-membered sharing face of $W_2@Li_{18}$ (18.A); 17. A is so stable that it can be obtained through the reoptimization of other low-energy isomers. This may be due to the lightest metal lithium atom with a fluxional behavior and the high stability of its $W@Li_{12}$ monomer (Table S1). Interestingly, the 17.A isomer has a magnetic moment of 1 μ_B in spite of its nonmagnetic monomer, which will further enhance its stability.

3.5 | $W_2@Li_{16}$

The global minimum of the $W_2@Li_{16}$ (16.A) isomer continues the five-membered face-sharing feature, and it can be obtained by removing one lithium atom from any of the endmost five-atom rings of $W_2@Li_{17}$ (17.A). Removing a lithium atom from a top atom or the middle five-membered ring of 17.A, the isomers of 16.B and 16.D are formed accordingly. Both of them are less stable than 16.A with a relative energy of 0.08 and 0.56 eV, respectively. The isomer 16.C is 0.53 eV higher in energy, exhibiting a relatively compact structure.

3.6 | $W_2@Li_{15}$

Similar to 17.A and 16.A, the ground-state structure of $W_2@Li_{15}$ (15.A) persists in the five-membered motif. Apparently, its formation can be accounted by removing the top lithium atom from the sparse side of $W_2@Li_{16}$ (16.A). Two more symmetrical isomers of 15.B and 15.C, both with an energy of 0.42 eV higher than 15.A, can be formed by a lithium atom removed from the marginal five-membered ring of 16.A or two top lithium atoms detached from 17.A. The structural style of the C_{2v} symmetry 15.D has a close relation to 16.C, of which the capping atoms are two pairs of symmetry-equivalent lithium atoms, and 15.D can be obtained by a single lithium atom replacement of each at their average position.

3.7 | $W_2@Li_{14}$

Despite continually removing a lithium atom, the two W atoms are not completely encapsulated by the Li_{14} cage in the global minimum isomer of $W_2@Li_{14}$ (14.A). Obviously, 14.A is incapable of a superatomic molecule. For the second isomer, 14.B, its energy is higher by about 0.25 eV, evolved from 16.C or 15.D with their paired capping lithium atoms being replaced. The next two isomers of 14.C and 14.D are less stable at about 0.27 and 0.39 eV, respectively, and also have a cage-like structure.

With the size decreasing, it should be noted that the bond lengths of W and W are successively elongated, increasing from $W_2@Li_{20}$ (2.519 Å) to $W_2@Li_{18}$ and then a decreasing thereafter, whereas the changes in the middle sharing Li ring are the reverse, as shown in Table 1. The underlying reasons can be conjectured from their structural evolutions. For $W_2@Li_{20}$, the face-sharing bi-superatomic configuration is metastable, as found in our previous study,[14] of which one Li atom was removed from its six-membered Li ring located at any end, and the obtained isomer of $W_2@Li_{19}$ is the global minima and possesses the properties of superatomic molecules. The same occurs in $W_2@Li_{18}$—both removed Li atoms from the terminal six-membered Li rings. Meanwhile, the repulsion of the intermediate six-membered Li ring to W atoms is observed due to the reduced counteracted interactions from the terminal, and thus, the two W atoms are far away. For $W_2@Li_n$ (n = 15-17), the distances of W and W are shortened to a large extent due to a shortage of lithium atoms. The distribution of lithium atoms clearly demonstrates that one half is more compact than the other half, and a WLi_{12} is retained throughout. In other words, two W atoms are fighting over lithium atoms to keep themselves more compact, and a W atom could handle some coordination to form a core-shell structure. The sites that are severely deficient in Li atoms will be compensated by the W atoms, leading to the distances of two W closed atoms. This phenomenon can be further understood by the stability of their monomers. Based on the jellium model, both the 18-electron and 20-electron systems are stable. However, a Ti atom or its same main group elements of Zr and Hf doped into Li clusters, the corresponding most stable isomers are all with the centered cage-like shapes, whereas this geometric structure is retained doped by W atom other than Cr and Mo atoms among the VIB transition metal elements, predicting the robustness of an 18-electron monomer. In addition, the compact half with WLi_{12} monomers for $W_2@Li_n$ (n = 14-17) and the local maximum of E_f in $W_2@Li_{17}$ are indicative of the specific stability of the monomer and molecules.

3.8 | Relative stability of $W_2@Li_n$ (n = 14-19) clusters

According to the PSO searches and DFT calculations, the lowest-lying isomers of $W_2@Li_n$ (n = 14-19) maintain the structural motif by entirely enclosing two W atoms into Li_n cages, except $W_2@Li_{14}$. To further probe their stability, two quantities, namely, the average binding energy (E_b) and the fragmentation energy (E_f), of the isomers with global minimum ($W_2@Li_{14}$, 14.B) are evaluated, which can be sequentially defined as follows:

$$E_b(W_2@Li_n) = \frac{2E(W) + nE(Li) - E(W_2@Li_n)}{n+2}$$

$$E_f(W_2@Li_n) = E(W_2@Li_{n-1}) + E(Li) - E(W_2@Li_n)$$

TABLE 1 The calculated bond lengths (Å) of the most stable isomers for $W_2@Li_n$ (n = 15-19) at the level of PW91/SDD, where the signs of ⊥, //, × are relative to their axial direction of W and W

	Location	$W_2@Li_{19}$	$W_2@Li_{18}$	$W_2@Li_{17}$	$W_2@Li_{16}$	$W_2@Li_{15}$
Li-$Li_{\perp}$	middle	2.483-2.662	2.382-2.741	2.817-2.981	2.813-3.034	2.852-3.074
	end(sparse)	2.822-2.912	2.808-2.937	2.894-2.911	3.039-3.125	3.002-3.156
	end	2.647-2.686			2.891-2.943	2.912-2.956
Li-$Li_{//}$	end(sparse)	2.896-2.927	2.832-3.011	2.924-2.948	2.821-2.850	-
	end	3.067-3.134			2.928-2.948	2.932-2.970
Li-$Li_{\times}$	sparse	2.767-3.163	2.696-3.078	2.957-3.049	2.968-3.091	3.019-3.177
	inc	2.907-2.961			2.997-3.067	3.036-3.098
Li-$W_{//}$	sparse	3.028	2.980	2.925	3.176	-
	inc	2.819			2.915	2.867
Li-$W_{\times}$	sparse	2.776-2.947	2.743-2.845, 3.079	2.751-2.826	2.705-2.807	3.019-3.177
	inc	2.861-2.956			2.761-2.823	3.036-3.098
W-W	-	2.535	2.552	2.512	2.458	2.399

Here, the range of n is from 14 to 19. E(Li) or E(W), E(W_2@Li_n), and E(W_2@Li_{n-1}) denote the total energy of a free Li or W atom, a W_2@Li_n cluster, and a W_2@Li_{n-1} cluster, respectively.

As shown in Figure S3, E_b is a monotone decreasing function of n for the ground states of W_2@Li_n (n = 14-19), indicating that the stability is reduced with the size increase. In other words, the cage-like shell isomers centered by a W dimer exhibit no advantage in energy with the increased number of Li atoms, and W_2@Li_{20} is such an example, for which the total energy of the superatomic molecule is 0.08 eV higher than that of the lowest-lying isomer with a noncage shape. E_f denotes gain in energy as a successive addition of an Li atom to the preceding size W_2@Li_{n-1}. Note that there are two conspicuous maxima of E_f for W_2@Li_n clusters at n = 17 and 15, indicating that W_2@Li_{17} and W_2@Li_{15} are particularly stable compared with their neighbors. The underlying reasons may respectively be attributed to the high stability of monomer (Table S1) and a high magnetic moment of 3 μ_B for W_2@Li_{17} and W_2@Li_{15}. Besides, an energy gap of the highest occupied molecular orbital (HOMO) and the lowest unoccupied molecular orbital (LUMO) is examined, where a large HOMO-LOMO gap will enhance the stability.[26,27] The variation of E_{gap} in the W_2@Li_n clusters shows that the lowest-lying isomer of W_2@Li_{15} has the largest gap of 0.49 eV (PW91/SDD) in the series, corresponding to its high stability. The gaps of other isomers are moderate in comparison with that of the typical magnetic superatoms, such as V@Na_8 (0.69 eV),[5] $MnSr_9$ (0.35 eV),[28] and VNa_8^- (0.42 eV).[6]

To evaluate the feasibility of the two W atoms encapsulated in the Li cage, the interaction of the embedded atoms and the outer cage, namely, the embedding energy (D_e), is calculated using the following equation

$$D_e(W_2@Li_n) = E(\text{shell}) + E(\text{core}) - E(W_2@Li_n)$$

where E(shell), E(core), and E(W_2@Li_n) respectively represent the total energies of the Li_n cage, two W atoms, and the whole clusters. A positive D_e means that enclosing the two W atoms into the Li_n cage is practical, and the largest D_e value of W_2@Li_{17} indicates that its production process is the most favorable.

3.9 | Electronic structures and bonding analysis in W_2@Li_n (n.A, n = 15-19) clusters

The lowest-lying W_2@Li_{14} are found without cage-like geometric structures, and thus, there is no further discussion given here. To rationalize the prolate shapes and higher relative stability of W_2@Li_n (n.A, n = 15-19), their MOs and chemical bonding patterns are analyzed on the basis of the SVB model.

Figure 3 gives the MOs of lowest-energy W_2@Li_n (n = 15-19) isomers, and their electronic configurations are summarized in Table 2 for simplicity. The bonding/antibonding combination of two sets of MOs (σ_{1S} and σ^*_{1S}), two doubly degenerate sets of MOs ($\pi_{1Px,Py}$ and $\pi^*_{1Px,Py}$), and two sets of MOs (σ_{1Pz} and σ^*_{1Pz}) are derived from the interaction of 1S + 1S and 1P + 1P superatomic orbitals (SAOs). The two doubly degenerate sets of MOs ($\pi_{1Dxz,yz}$ and $\pi^*_{1Dxz,yz}$ [unlabeled]), two sets of MOs (σ_{1Dz2} and σ^*_{1Dz2} [unlabeled]), and two doubly degenerate sets of MOs ($\delta_{1Dx2\text{-}y2,xy}$ and $\delta^*_{1Dx2\text{-}y2,xy}$) correspond to the interacting 1D + 1D SAOs. For W_2@Li_{19} (19.A), the last occupied orbital σ_{2S} is given in terms of the interacting 2S + 2S SAOs. Owing to a lithium atom and a tungsten atom respectively offering one ($2s^1$) and six ($6s^25d^4$) effective valence electrons (ve), the filling order of 31-ve W_2@Li_{19} is $(\sigma_{1S})^2(\sigma^*_{1S})^2(\pi_{1Dxz,yz})^4(\sigma_{1Dz2})^2(\pi_{1Px,1Py})^4(\delta_{1Dx2\text{-}y2,xy})^4(\pi^*_{1Px,1Py})^4(\sigma_{1Pz})^2(\sigma^*_{1Pz})^2(\delta^*_{1Dx2\text{-}y2,xy})^4(\sigma_{2S})_\alpha^1(\sigma^*_{2S})_\beta^0$. Only one electron is unpaired, and W_2@Li_{19} has a magnetic moment of 1 μ_B. For calculation of the TPSSH/SDD level, its HOMO-LUMO energy gap is 0.65 eV, formed by the energy difference of $(\sigma_{2S})_\alpha$ and $(\sigma^*_{2S})_\beta$. The electronic configuration of 30-ve W_2@Li_{18} isomer (18.A) is in complete agreement with that of W_2@Li_{19}, except for the unfilled orbital σ_{2S}. Therefore, it is nonmagnetic. The energy difference of two doubly degenerate $\delta^*_{1Dx2\text{-}y2,xy}$ and σ_{2S} forms its energy gap of 0.82 eV. For 29-ve W_2@Li_{17} isomer (17.A), its electronic configuration is $(\sigma_{1S})^2(\sigma^*_{1S})^2(\pi_{1Dxz,yz})^4(\sigma_{1Dz2})^2(\delta_{1Dx2\text{-}y2,xy})_\alpha^1(\pi_{1Px,1Py})_\alpha^2(\delta_{1Dx2\text{-}y2,xy})_\alpha^1(\pi_{1Px,1Py})_\beta^2(\delta_{1Dx2\text{-}y2,xy})_\beta^2(\pi^*_{1Px,1Py})^4(\sigma_{1Pz})^2(\sigma^*_{1Pz})^2(\delta^*_{1Dx2\text{-}y2,xy})_\alpha^2(\delta^*_{1Dx2\text{-}y2,xy})_\beta^1(\sigma_{2S})^0$. In comparison with W_2@Li_{18} and W_2@Li_{19}, the $(\delta_{1Dx2\text{-}y2,xy})_\alpha$ MO energy level of 17.A is lower, which may have originated in its structural incompactness that leads to the interaction between two strengthened W atoms. The partially filled orbital $\delta_{1Dx2\text{-}y2,xy}$ forms its energy gap. The same occurs in 28-ve W_2@Li_{16} isomer (16.A) along with an electronic shell of $(\sigma_{1S})^2(\sigma^*_{1S})^2(\pi_{1Dxz,yz})^4(\sigma_{1Dz2})^2(\delta_{1Dx2\text{-}y2,xy})_\alpha^2(\pi_{1Px,1Py})_\beta^2(\pi_{1Px,1Py})_\alpha^2(\delta_{1Dx2\text{-}y2,xy})_\beta^2(\pi^*_{1Px,1Py})_\alpha^2(\sigma_{1Pz})_\beta^1(\sigma_{1Pz})_\alpha^1(\pi^*_{1Px,1Py})_\beta^2(\sigma^*_{1Pz})^2(\delta^*_{1Dx2\text{-}y2,xy})_\alpha^2(\delta^*_{1Dx2\text{-}y2,xy})_\beta^0$, and one more ve appears in its lower $(\delta_{1Dx2\text{-}y2,xy})_\alpha$ MO energy level. The stability of W_2@Li_{16} (16.A) is obtained by a magnetic moment of 2 μ_B and a second energy gap of all the lowest-lying isomers. Successively removing an Li atom, the geometric structure of 27-ve W_2@Li_{15} isomer (15.A) becomes looser and undergoes a bigger distortion. The electronic shell is $(\sigma_{1S})^2(\sigma^*_{1S})^2(\pi_{1Dxz,yz})^4(\sigma_{1Dz2})^2(\delta_{1Dx2\text{-}y2,xy})_\alpha^2(\pi_{1Px,1Py})^4(\delta_{1Dx2\text{-}y2,xy})_\beta^2(\pi^*_{1Px,1Py})_\alpha^2(\sigma_{1Pz})_\alpha^1(\pi^*_{1Px,1Py})_\beta^2(\sigma^*_{1Pz})_\alpha^1(\sigma_{1Pz})_\beta^1(\delta^*_{1Dx2\text{-}y2,xy})_\alpha^2(\sigma^*_{1Pz})_\beta^0(\delta^*_{1Dx2\text{-}y2,xy})_\beta^0$, where the location of $(\sigma_{1Pz})_\beta$ MO energy level is higher maybe due to a top lithium atom removed. A magnetic moment of 3 μ_B is formed to stabilize itself, and the largest energy gap of the series further enhances its stability. From the analysis of their canonical MOs, these n.A isomers (n = 15-19) can be viewed as superatomic molecules, which are formed by two homo- or heterosuperatoms.

Furthermore, the bonding characteristics of W_2@Li_n (n = 15-19) are probed by the adaptive natural density partitioning (AdNDP) method,[29] where the electron pair accounts for the chemical bonding models, including lone pairs (2c-2e [2-center 2-electron] and 1c-2e) and multicenter delocalized bonds (nc-2e). As expected, W_2@Li_{19} (19.A) possesses six multicenter (14c-2e or 15c-2e) super lone pairs (LPs) (super S, P_{xyz}, and $D_{x2\text{-}y2,xy}$), belonging to each superatom ($1S^21P^61D^4_{x2\text{-}y2,xy}$), and four 21c-2e superatom-superatom bonds (2σ, 2π) spread over the whole system.

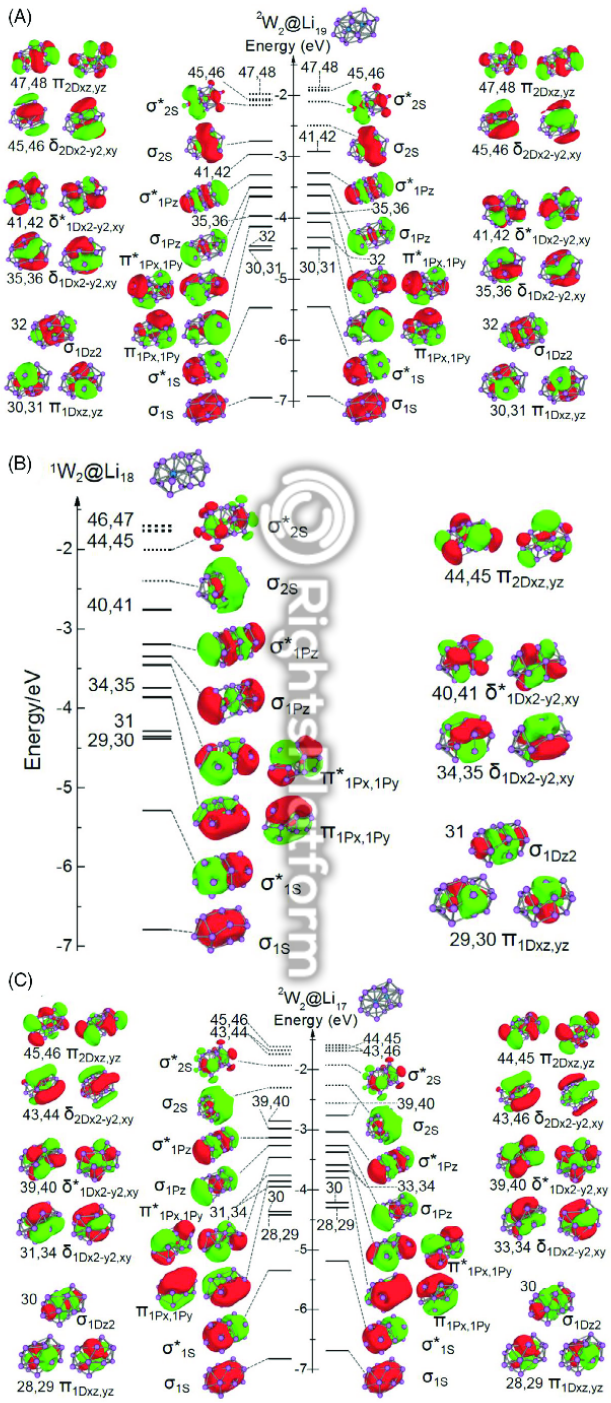

FIGURE 3 The canonical molecular orbitals of lowest isomers W_2Li_n (n = 15-19) calculated by PW91/SDD. The occupied levels are denoted by continuous lines, whereas the unfilled states are corresponding to the dotted lines. For clarity, the Kohn-Sham MOs are generated from the interaction of D + D shells marked with numbers

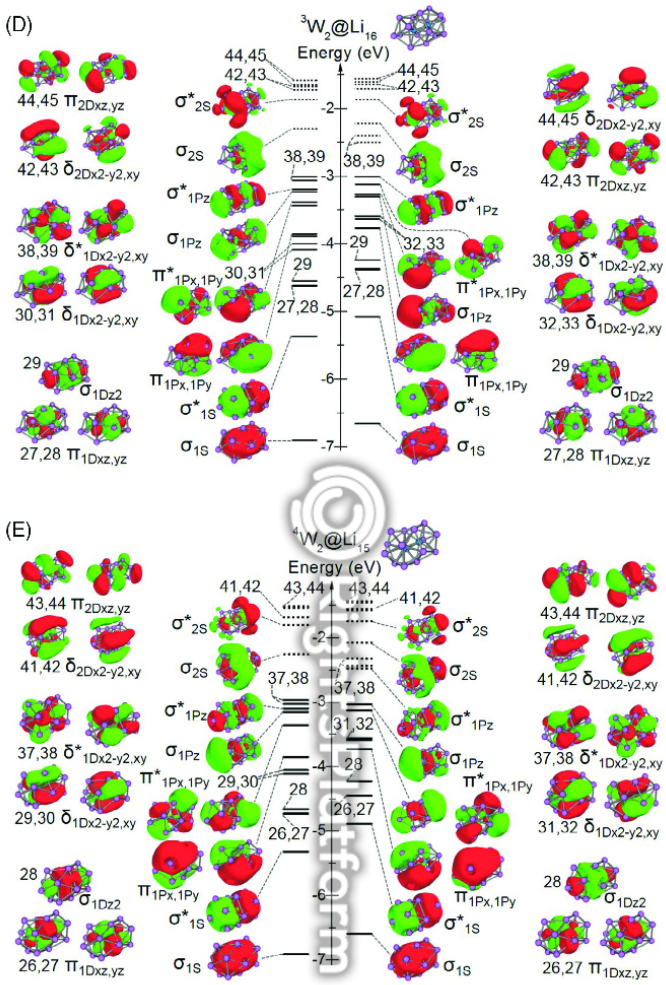

FIGURE 3 (Continued)

TABLE 2 The calculated symmetry, electron configuration, valence electrons (ve), and the total magnetic moment (μ_s) for $W_2@Li_n$ (*n*.A, *n* = 15-19) at the PW91/SDD level

System	Symm.	Electron configuration	ve	μ_s
$W_2@Li_{19}$	C_s	$(\sigma_{1S})^2(\sigma^*_{1S})^2(\pi_{1Dxz,yz})^4(\sigma_{1Dz2})^2(\pi_{1Px,1Py})^4(\delta_{1Dx2-y2,xy})^4(\pi^*_{1Px,1Py})^4(\sigma_{1Pz})^2(\sigma^*_{1Pz})^2(\delta^*_{1Dx2-y2,xy})^4\mathbf{(\sigma_{2S})_\alpha{}^1(\sigma^*_{2S})_\beta{}^0}$	31	1
$W_2@Li_{18}$	C_2	$(\sigma_{1S})^2(\sigma^*_{1S})^2(\pi_{1Dxz,yz})^4(\sigma_{1Dz2})^2(\pi_{1Px,1Py})^4(\delta_{1Dx2-y2,xy})^4(\pi^*_{1Px,1Py})^4(\sigma_{1Pz})^2(\sigma^*_{1Pz})^2\mathbf{(\delta^*_{1Dx2-y2,xy})^4(\sigma_{2S})^0}$	30	0
$W_2@Li_{17}$	C_{2v}	$(\sigma_{1S})^2(\sigma^*_{1S})^2(\pi_{1Dxz,yz})^4(\sigma_{1Dz2})^2(\delta_{1Dx2-y2,xy})_\alpha{}^1(\pi_{1Px,1Py})^4(\delta_{1Dx2-y2,xy})_\alpha{}^1(\delta_{1Dx2-y2,xy})_\beta{}^2(\pi^*_{1Px,1Py})^4(\sigma_{1Pz})^2(\sigma^*_{1Pz})^2$ $(\delta^*_{1Dx2-y2,xy})_\alpha{}^2\mathbf{(\delta^*_{1Dx2-y2,xy})_\beta{}^1(\sigma_{2S})^0}$	29	1
$W_2@Li_{16}$	C_s	$(\sigma_{1S})^2(\sigma^*_{1S})^2(\pi_{1Dxz,yz})^4(\sigma_{1Dz2})^2(\delta_{1Dx2-y2,xy})_\alpha{}^2(\pi_{1Px,1Py})^4(\delta_{1Dx2-y2,xy})_\beta{}^2(\pi^*_{1Px,1Py})_\alpha{}^2(\sigma_{1Pz})^2(\pi^*_{1Px,1Py})_\beta{}^2(\sigma^*_{1Pz})^2$ $\mathbf{(\delta^*_{1Dx2-y2,xy})_\alpha{}^2(\delta^*_{1Dx2-y2,xy})_\beta{}^0}$	28	2
$W_2@Li_{15}$	C_s	$(\sigma_{1S})^2(\sigma^*_{1S})^2(\pi_{1Dxz,yz})^4(\sigma_{1Dz2})^2(\delta_{1Dx2-y2,xy})_\alpha{}^2(\pi_{1Px,1Py})^4(\delta_{1Dx2-y2,xy})_\beta{}^2(\pi^*_{1Px,1Py})_\alpha{}^2$ $(\sigma_{1Pz})_\alpha{}^1(\pi^*_{1Px,1Py})_\beta{}^2\mathbf{(\sigma^*_{1Pz})_\alpha{}^1(\sigma_{1Pz})_\beta{}^1(\delta^*_{1Dx2-y2,xy})_\alpha{}^2(\sigma^*_{1Pz})_\beta{}^0(\delta^*_{1Dx2-y2,xy})_\beta{}^0}$	27	3

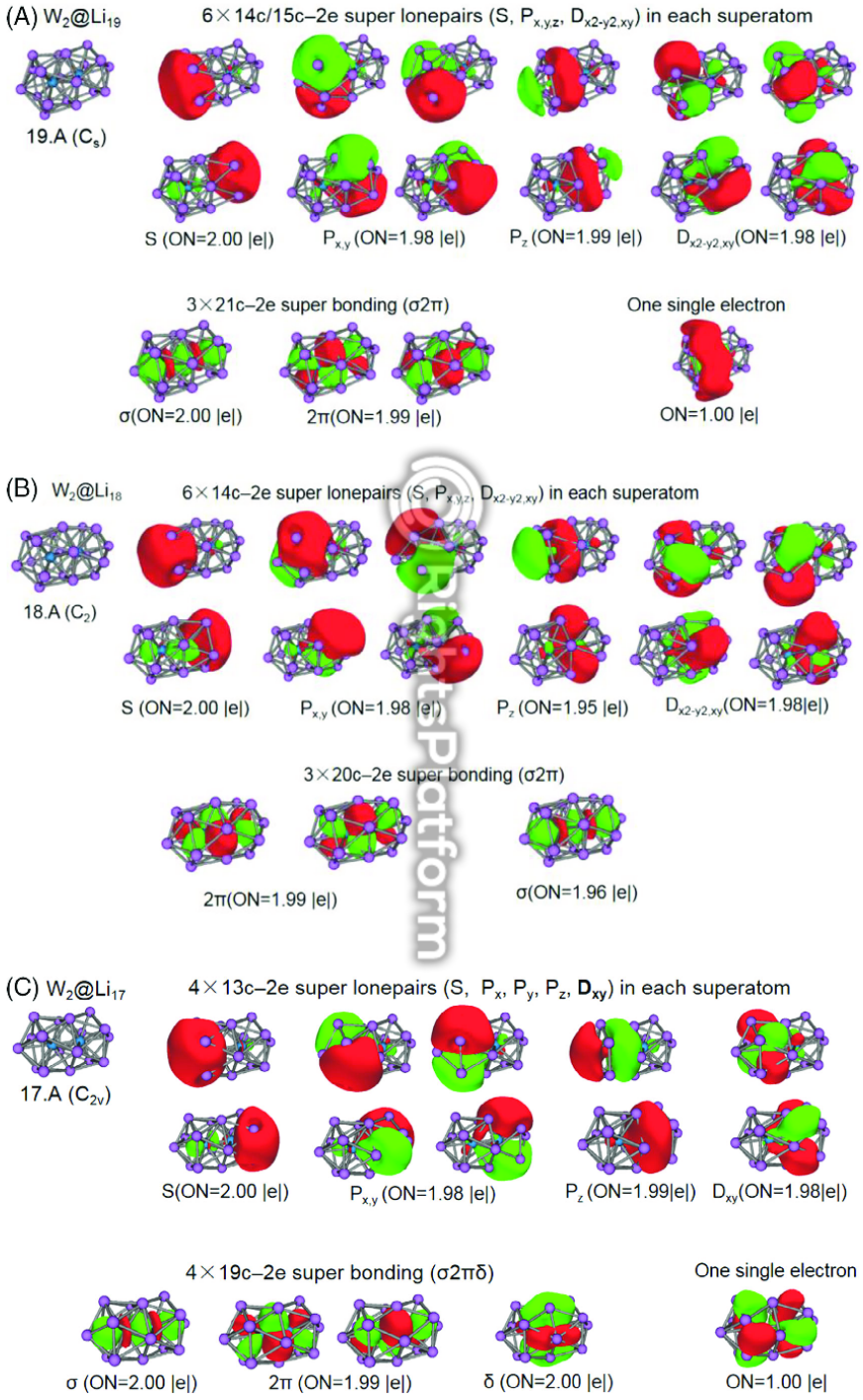

FIGURE 4 Geometric structures and AdNDP bonding patterns of *n*.A for W_2Li_n (*n* = 15-19) clusters. AdNDP, adaptive natural density partitioning

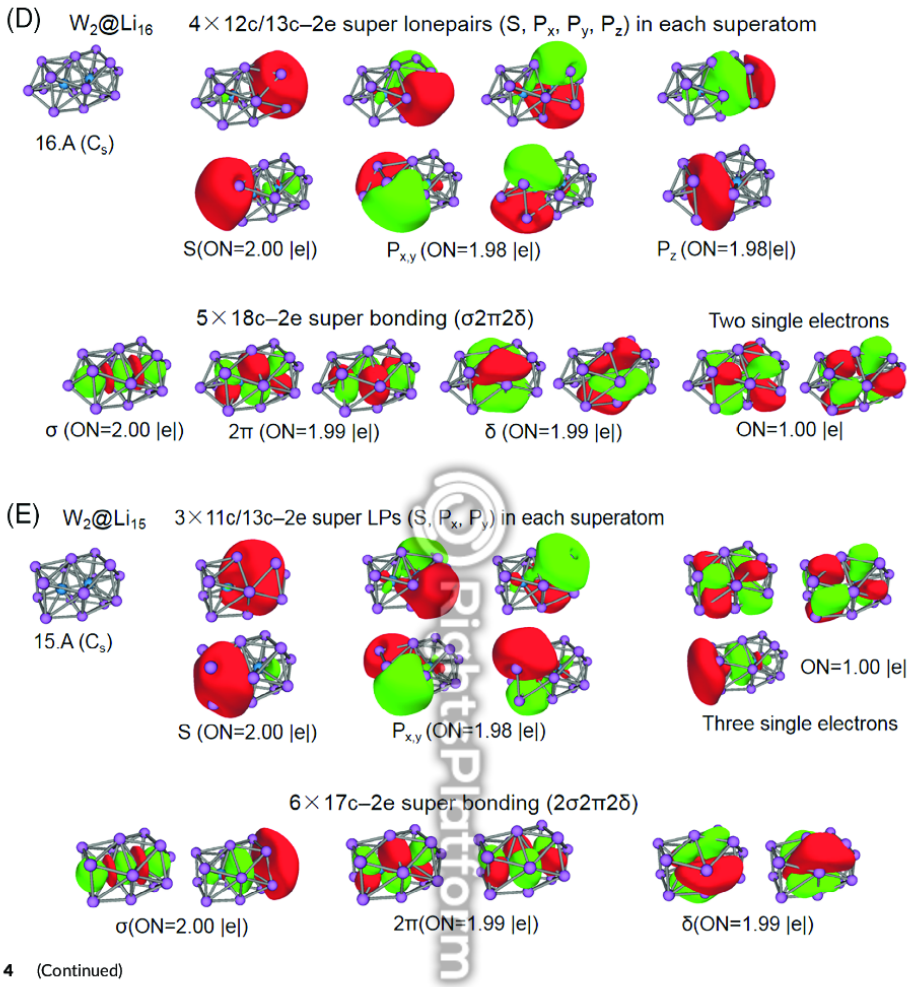

FIGURE 4 (Continued)

Due to the unpaired orbital σ_{2S}, its super bond order is 3.5. A similar bonding pattern occurs in $W_2@Li_{18}$ (18.A). As a result of the removed electron from orbital σ_{2S}, its super bond order becomes 3, and there exists three delocalized superatom-superatom bonds of 20c-2e (σ, 2π). For $W_2@Li_{17}$ (17.A), the partially occupied orbital $\delta^*_{1Dx2\text{-}y2,xy}$ of β leads to an increscent bond order of 3.5 and four 19c-2e superatom-superatom bonds (σ, 2π, δ). Based on a decrease by one more $\delta^*_{1Dx2\text{-}y2,xy}$ orbital β electron, the super bond order of $W_2@Li_{16}$ (16.A) increases again to 4, and five 18c-2e super bonding (σ, 2π, 2δ) exists. Despite continually removing an Li atom, the reduced effective ve is still sequentially derived from the antibonding orbitals of β. Hence, the super bond order of $W_2@Li_{15}$ (15.A) is 4.5, and there are six 17c-2e superatom-superatom bonds (2σ, 2π, 2δ). The occupation number (ON) of all the described bonds is 1.95 to 2.00 |e|, indicating the reliability of the AdNDP bonding analysis (Figure 4).

Both the analysis of the MO shapes and the AdNDP bonding patterns reveal that the most stable isomers of $W_2@Li_n$ (n = 15-19) possess characteristics of superatomic molecules. The total and partial density of states for such series are shown in Figure 5 to determine the ingredients of bonds, where the energy levels are broadened by Gaussians of a width of 0.12 eV. It can been seen that the atomic composition of the density of states are quite similar. The lowest two states σ_{1S} and σ^*_{1S} are composed mainly of s (Li and W) atomic orbitals (AOs), while the essential ingredients for $\pi_{1Px,Py}$, σ_{1Pz}, $\pi_{1Dxz,yz}$, σ_{1Dz2}, and their anti-bond states are s (Li) and p (W) AOs. All these states have a larger component of the d (W) AOs. As for $\delta_{1Dx2\text{-}y2,xy}$ and $\delta^*_{1Dx2\text{-}y2,xy}$, they are contributed by s (Li) and d (W) AOs. The introduce of transition metal atoms may aid in developing stable magnetic clusters and the formation of δ-bonds. The existence of isosupermolecules among the low-energy structures offers various assembly patterns from superatoms, which will further approach the prospect of cluster-assembled materials with tailored properties.